Proximal mutations at the type 1 copper site of CotA-Laccase; spectroscopic, redox, kinetic and structural characterization of I494A and L386A mutants

Paulo Durao, Zhenjia Chen, Catarina S Silva, Cláudio M Soares, Manuela M Pereira, Smilja Todorovic, Peter Hildebrandt, Isabel Bento, Peter F Lindley, Lígia O Martins

Proximal Mutations at the Type 1 Copper Site of CotA-Laccase; Spectroscopic, Redox, Kinetic and Structural Characterization of I494A and L386A mutants

Paulo Durão[*], Zhenjia Chen[*], Catarina S. Silva[*], Cláudio M. Soares[*], Manuela M. Pereira[*], Smilja Todorovic[*], Peter Hildebrandt[†], Isabel Bento[*], Peter F. Lindley[*] and Lígia O. Martins[*]

[*]*Instituto de Tecnologia Química e Biológica, Universidade Nova de Lisboa, Av. da República, 2781-901 Oeiras, Portugal.*

[†]*Technische Universität Berlin, Institut für Chemie, Sekr. PC 14, Straße des 17. Juni 135, D-10623 Berlin, Germany.*

Running title: Laccase T1 Cu Site Mutations.

Key words: laccase, multicopper oxidase, T1 Cu, site-directed mutagenesis, CotA-laccase

Corresponding Author: lmartins@itqb.unl.pt, Telf: +351 214469534, Fax: +351 214411277

ABSTRACT

The CotA-laccase from *Bacillus subtilis* has been mutated at two hydrophobic residues in the vicinity of the type 1 Cu site. The mutation leucine 386 to alanine appears to cause only very subtle alterations in the properties of the enzyme indicating minimal changes in the structure of the Cu centres. However, the replacement of isoleucine 494 by an alanine leads to significant changes in the enzyme. Thus, the major visible absorption band is up-shifted by 16 nm to 625 nm and exhibits an increased intensity, whilst the intensity of the shoulder at ca. 330 nm is decreased by a factor of two. Simulation of the EPR spectrum of the I494A mutant reveals differences in the type 1 as well as in the type 2 centre reflecting modifications of the geometry of these centres. The intensity weighted frequencies $<\nu_{Cu-S}>$, calculated from Resonance Raman spectra are 410 cm^{-1} for the Wt enzyme and 396 cm^{-1} for the I494A mutant, indicating an increase of the Cu-S bond length in the type 1 Cu site of the mutant. Overall the data clearly indicate that the I494 mutation causes a major alteration of the structure near the type 1 Cu site and this has been confirmed by X-ray crystallography. The crystal structure shows the presence of a fifth ligand, a solvent molecule, at the type 1 Cu site leading to an approximate trigonal bipyramidal geometry. The redox potential of the L386A and I494A are shifted downwards by about 60 and 100 mV, respectively. These changes correlate well with decreased catalytic efficiency of both mutants compared with the Wt.

INTRODUCTION

Laccases are the simplest members of the multi-copper oxidase (MCO) family of enzymes that includes ascorbate oxidase (L-ascorbate oxygen oxidoreductase, EC 1.10.3.3) and ceruloplasmin (Fe(II) oxygen oxidoreductase, EC 1.16.3.1). MCOs are characterized by having four Cu(II) ions that are classified into three distinct types of Cu sites, namely type 1 (T1), type 2 (T2) and type 3 (T3) [1-4]. The classical T1 Cu site comprises two histidine residues and a cysteine arranged in a distorted trigonal geometry around the Cu ion with bonding distances around 2.0 Å; a weaker fourth methionine ligand completes the tetrahedral geometry with a Cu-S distance of about 3.2 Å. The Cu-Cys linkage is characterized by an intense $S(\pi) \rightarrow Cu(d_{x^2-y^2})$ charge transfer (CT) absorption band at around 600 nm, the origin of an intense blue colour of these enzymes, and a narrow parallel hyperfine splitting [$A_{\parallel}$ = (43-90) x 10^{-4} cm^{-1}] in the electron paramagnetic resonance spectrum (EPR). Upon excitation into the CT band, the resonance Raman (RR) spectra of blue copper proteins typically display several bands between 350 and 430 cm^{-1} involving the Cu-S(Cys) stretching coordinates. The intensity weighted frequency average of these modes allows estimating the Cu-S bond length and thus provides insight into the T1 site geometry [5]. The function of the T1 Cu site is to shuttle electrons from substrates (via one of the histidine ligands oriented towards the molecular surface) to the trinuclear Cu centre where molecular oxygen is reduced to two molecules of water during the complete 4-electron catalytic cycle. The trinuclear centre contains a T2 Cu coordinated by two histidines and one water molecule, lacks strong absorption bands and exhibits a large parallel hyperfine splitting in the EPR spectrum [$A_{\parallel}$ = (150-201) x 10^{-4} cm^{-1}]. The T2 Cu site is in close proximity to two T3 Cu ions, which are each coordinated by three histidines and typically coupled, for example, through a hydroxide bridge. The T3 or coupled binuclear Cu site is characterized by an intense absorption band at 330 nm originating from the bridging ligand and by the absence of an EPR signal due to the antiferromagnetically coupling of the Cu ions.

The catalytic rate-limiting step in laccases is considered to be the oxidation of the substrate at the T1 Cu site, which switches between the +1 and +2 redox states [1]. The reduction potential of the Cu(II)/Cu(I) couple is thus a crucial physico-chemical parameter for the enzyme function. Understanding the molecular factors such as Cu ligation pattern, the polarity of the protein environment, and the solvent accessibility of the metal site, responsible for its modulation is of utmost importance. Several studies have demonstrated that a weak axial bond at the T1 Cu site preferentially destabilizes the oxidized state, and is therefore, a key factor for the high reduction potentials (400-700 mV) of blue Cu sites in MCOs [1]. In a previous work we have shown that the replacement of M502 (weakly coordinating to the T1 Cu) in CotA-laccase by the non-coordinating residues leucine and phenylalanine allowed the maintenance of the T1 Cu geometry while causing an increase in the redox potential by ~100 mV [6]. Nevertheless, mutations of the axial ligand have a profound impact on the thermodynamic stability of the enzyme and no direct correlation was found between the redox potentials and the oxidation rates of the enzyme, as lower turnover rates were measured for both mutants. In this work site-directed mutagenesis has been used to replace the residues I494 and the L386 in the CotA laccase by alanine in order to change the hydrophobic environment of the T1 Cu site, namely the hydrophobic patch surrounding its H497 ligand (Figure 1). This latter residue is exposed to the solvent and is presumably involved in the electron transfer pathway from reduced substrates to T1 Cu [8]. The effects of the replacements of hydrophobic I494 and L386 on the T1 Cu of CotA-laccase have been examined by various spectroscopic techniques (UV-visible, EPR and RR) and by X-ray

crystallography. In the case of the L386A mutant, two crystal structures have been evaluated, one for a "fully loaded" copper sample at the medium resolution of 2.9Å and the second for a sample significantly depleted in T2 and T3 copper ions, but at an improved resolution of 2.4 Å. The results obtained from all these different techniques allowed for elucidation of the impact of the mutations on the redox and kinetic properties of the enzyme.

MATERIAL AND METHODS

Construction of CotA mutants. Single amino acid substitutions in the T1 Cu centre were created using the QuickChange site-directed mutagenesis kit (Stratagene). Plasmid pLOM10 (containing the Wt CotA sequence) was used as a template [9]. The primers, forward 5'- CGT ATG GCA TTG CCA TGC TCT AGA GCA TGA AGA C -3' and reverse 5'- GTC TTC ATG CTC TAG AAG CAT GGC AAT GCC ATA CG -3' were used to generate the I494A mutant whereas the primers, forward 5'- CGG CAG ACC CGT CGC TCT GCT TAA TAA CAA ACG C -3' and reverse 5'- GCG TTT GTT ATT AAG CAG AGC GAC GGG TCT GC -3' were used to generate the L386A mutation. The presence of the desired mutations in the resulting plasmids, pLOM27 (carrying the I494A point mutation) and pLOM15 (bearing the L396A point mutation) and the absence of unwanted mutations in other regions of the insert were confirmed by DNA sequence analysis. Plasmids pLOM27 and pLOM15 were transformed into *Escherichia coli* Tuner (DE3) strains (Novagen) to obtain strains AH3547 and AH3560, respectively.

Overproduction and purification. Strains AH3517 (containing pLOM10), AH3547 and AH3560 were grown in Luria–Bertani medium supplemented with ampicillin (100 µg/mL) at 30ºC. Growth was followed until the midlog phase (OD_{600}=0.6), at which time 0.1 mM isopropyl-β-D-thiogalactopyranoside and 0.25 mM $CuCl_2$ were added to the culture medium. The temperature was changed to 25ºC and agitation maintained for 4 h. The agitation was then interrupted and the cells were maintained overnight at the same temperature. Such a protocol leads to a maximum occupancy of the Cu sites [10]. Mutants prepared by this protocol will be referred to as "fully loaded". In a previous protocol involving overnight shaking [9] significant Cu depletion was observed in both the T2 and T3 sites and the sample of L386A mutant prepared in this manner will be referred as "Cu depleted". Cell harvesting and disruption and protein purification using a two-step protocol procedure were undertaken as previously described [7, 9]. Purified enzymes were stored at -20ºC until use.

UV-Visible, EPR, RR spectra. UV-visible spectra were acquired using a Nicolet Evolution 300 spectrophotometer from Thermo Industries. EPR spectra were measured with a Bruker EMX spectrometer equipped with an Oxford Instruments ESR-900 continuous-flow helium cryostat. The spectra obtained under non-saturating conditions (160 µM protein content) were theoretically simulated using the Aasa and Vänngard approach [11]. RR spectra were measured from the frozen sample (-190ºC) using confocal spectrograph (Jobin Yvon, XY) equipped with grating of 1800 lines/ mm and a liquid nitrogen cooled back illuminated CCD camera. For excitation, the 567.9-nm line of a Kr^+ laser (Coherent, Innova 300K), laser power of 5 mW at the sample, was used. Typical accumulation times were 40 s. About 2 µL of 1 mM 'as purified' oxidized CotA, I494A and L386A mutants (in 20 mM Tris buffer, pH 7.6) were introduced into a liquid nitrogen cooled cold finger (Linkam THMS600) mounted on a microscope stage. The RR spectra (350-450 cm^{-1} region) were submitted to band fitting analysis using Lorentzian

bandshapes. The fitted band intensities and frequencies were used for determination of the intensity weighted frequency $<\nu_{Cu-S}>$ [5].

Redox titrations and enzyme assays. Redox titrations were performed at 25ºC, and pH 7.6, under an argon atmosphere, and monitored by UV-vis spectroscopy (300-900 nm), using a Shimadzu Multispec-1501 spectrophotometer as described by Durão *et al* [6]. The laccase-catalysed oxidation reactions of ABTS, 2,6-dimethoxyphenol (2,6-DMP) and syringaldazine (SGZ) were photometrically monitored, as previously described [6]. Kinetic data were determined from Lineweaver–Burk plots assuming that simple Michaelis–Menten kinetics was followed. The reaction mixtures contained ABTS (10–240 µM, pH 4), 2,6-DMP (10-1000 µM, at pH 7 for Wt and L386A mutant or 100-7500 µM or at pH 9 for I494A mutant) or SGZ (1-100 µM, at pH 7 for Wt and L386A mutant or at pH 8 for I494A mutant). All enzymatic assays were performed at least three times.

Crystallization. Crystals of the I494A mutant were obtained at room temperature from a crystallization solution containing 0.1 M sodium citrate, 10% PEG MME 5K and 14% isopropanol at pH 5.5. Pale blue hexagonal prisms appeared from a drop containing 10.8 mg/ml of protein. In a similar manner, crystals of the L386A mutants appeared at room temperature from a crystallization solution containing 20% PEG MME 5K, 0.1 M sodium citrate, 8% isopropanol, at pH 5.5 and a protein concentration of 7.9 mg/ml. Cryo conditions were provided by adding 22% ethylene glycol to the crystallisation solution or, in the case of the Cu depleted L386A crystals, 25% of glycerol.

X-ray Data collection and refinement. Data collection was performed at 100 K using synchrotron radiation at the European Synchrotron Radiation Facility, Grenoble, France and the Swiss Light Source at the Paul Scherrer Institut, Villigen, Switzerland. Data collection details are shown in Table 1. Data sets for the I494A and L386A mutant enzymes were processed with MOSFLM [12] and scaled with SCALA [13] from the CCP4 program suite [14]. The data set for the Cu depleted L386A mutant extended to a significantly higher resolution, 2.4 Å, compared to 2.9 Å for the fully loaded mutant and hence was included in this study. The structures were elucidated by molecular replacement using MOLREP [15]. The starting model was the CotA native structure (PDB code: 1w6l [7]) from which all the Cu ions and solvent atoms had been removed. In each case only one solution was evident. Subsequent electron density syntheses enabled the location of the 4 Cu ions in the molecule. Refinement was performed using the maximum likelihood functions implemented in REFMAC5 [16]. Rounds of conjugate-gradient sparse-matrix refinement with bulk-solvent modeling according to the Babinet principle [17] were alternated with model building using the Coot program suite [18] in combination with SigmaA weighted $2|F_o| - |F_c|$ and $|F_o| - |F_c|$ maps [19]. After the first rounds of refinement, solvent molecules were added to the models based on standard geometrical and chemical restraints; molecules of ethylene diol, used as a cryo-protectant, were also located. In all cases, in a similar manner to the Wt structure, the loop region between residues 89 and 97 was very poorly defined. The occupancies of the Cu ions were adjusted such that their isotropic thermal vibration parameters refined approximately to the values of their local environment. For the T2 Cu centre in particular, including the fully loaded mutants, assignment of full occupancy led to thermal vibration coefficients significantly higher than the local average and significant features in difference Fourier syntheses. Careful use of omit and standard difference Fourier syntheses, as well as monitoring of thermal vibration coefficients during refinement and modeling studies, enabled the identification of diatomic species in between the T3 Cu sites in all cases and this was

interpreted as a dioxygen type species: refinement proceeded constraining the O-O distances to a target value of 1.08 Å. Moreover, in both fully-loaded mutants, additional electron density was observed in the vicinity of Cys35 and this was modeled as an oxidized cysteine species occupying two distinct configurations. Details of the overall refinement and final quality of the models are shown in Table 1 in the Supplementary Data.

Simulation studies. Simulated redox titrations [20, 21] were performed for studying the equilibrium binding of protons and electrons. The methodology is based on continuum electrostatic (CE) methods and Monte-Carlo (MC) sampling of binding states. The CE calculations were performed using the package MEAD (version 2.2.0) [22, 23]. The sets of atomic radii and partial charges were taken from GROMOS96 [24, 25], except in the case of the metal centres, where quantum chemical calculations (see below) were used to derive charges. Dielectric constants of 80 and 10 were used for the solvent and protein, respectively, which are values within the range where pK_a prediction is optimised [26]. The solvent probe radius was 1.4 Å, the ion exclusion layer 2.0 Å, the ionic strength 0.1 M and the temperature 27ºC. The program PETIT [20, 21] was used for the MC sampling of proton and electron binding states. Site pairs were selected for double moves when at least one pairwise term was greater than 2 pK units. Averages were computed using 10^5 MC steps. In all simulations, the trinuclear centre was considered to be in the fully oxidised state, while the T1 Cu centre was considered as titrable. Redox titrations are usually relative due to the unavailability of an E_{mod}, i.e. the redox potential of an adequate model compound in water; this is the case for the T1 Cu centre. Due to this, the experimental value for the Wt enzyme was used to fit the redox titrations by adding a constant value to the potential so that the calculated and measured redox potentials for the Wt enzyme were the same. The values for the mutants were then obtained relatively to this. Partial charges for the two metal clusters (T1 Cu and the T2 and 3 Cu ions) were calculated considering model compounds with the conformation of the oxidised structure obtained previously [7]. The ligands of the metals were considered up to the C-beta carbon (C-alpha in the case of the cysteine residue of the T1 Cu). A dioxygen molecule bound to the T3 Cu ions was considered, as well as the water molecule bound to the T2 Cu. Single point calculations were performed using Gaussian 98 [27], with the B3LYP and the 6-31G(d) basis set for all atoms, with the exception of Cu atoms, for which the 6-31G(2df) basis set was used. These calculations were employed to derive electrostatic potentials, which were then fitted using RESP [28] to calculate the partial charges. For the T1 Cu, partial charges were calculated for the oxidised and reduced states, since both were required to simulate the redox titration of this group.

Other methods. Protein copper content was determined through the trichloroacetic acid/bicinchoninic acid method of Brenner and Harris [29]. The protein concentration was measured by using the absorption band of CotA-laccase at 280 nm (ε_{280}=84,739 M^{-1} cm^{-1}) or the Bradford assay [30] using bovine serum albumin as a standard.

RESULTS AND DISCUSSION

Spectroscopic analysis of mutant enzymes

Site-directed mutagenesis replacing residues I494 and L386 by alanine in the CotA laccase was undertaken in order to change the hydrophobic environment of the T1 Cu centre (Figure 1). The resulting mutant enzymes show the same chromatographic pattern during purification as the wild-type CotA laccase. Protein samples were judged to be homogeneous by the observation of a

single band on a Coomassie Blue stained sodium dodecyl sulphate polycralamide electrophoresis gel. Each protein "as isolated" contained approximately 4 moles of Cu per 1 mole protein (Table 2). Figures 2, 3 and 4 show the visible, RR and EPR spectral characteristics of the Wt enzyme and the L386A and I494A mutants. The spectroscopic analysis of L386A mutant reveals very subtle differences when compared with the Wt protein, indicating minimal changes in the structure of the Cu centres. On the other hand, the I494A mutant shows distinct changes in the absorption spectra such as a shift of the CT transition (T1 Cu site) from 609 nm to 625 nm, a more intense blue colour (ε of 5,600 instead of 4,000 mM^{-1} cm^{-1}) and a two fold decrease of the extinction of the 330 nm band (a transition characteristic of the T3 coupled Cu ions) (Figure 2 and Table 2). The RR spectra of the Wt CotA, and the I494A and L386A mutants, obtained with a 567.9 nm excitation at -190°C, display seven vibrational bands between 350 and 440 cm^{-1} (Figure 3). Overall, the spectra bear strong similarities with those of other copper proteins containing T1 blue Cu site [5, 31-35]. However, quite different intensity distribution among the various modes in the spectrum of the I494A mutant, as compared to the Wt protein and the L386A mutant (Figure 3), indicates a substantial perturbation of the T1 site geometry upon replacing I494 by alanine. Since excitation in the resonance with the CT transition predominantly provides enhancement to the modes through the Cu-S stretching coordinate, its contribution to the various modes can be considered to be directly related to the relative RR intensities. Consequently, the intensity-weighted band frequencies allow determining the intrinsic Cu-S stretching frequency, which is inversely proportional to Cu-S bond length and thus provides a quantitative basis for description of the structural perturbation of the T1 Cu site [5, 31-35]. The intensity-weighted band frequencies, obtained by a band fitting analysis, include only vibrational fundamentals below 500 cm^{-1}. The value for the intrinsic Cu-S stretching frequency $<\nu_{Cu\text{-}S}>$ was found to be 410 cm^{-1} for the Wt protein, whereas for the T1 Cu site of I494A it was substantially lower (396 cm^{-1}), corresponding to a lengthening of the Cu-S(Cys) bond for the latter. For the L386A mutant, a value very similar to the one determined for the Wt, $<\nu_{Cu\text{-}S}>$ = 408 cm^{-1}, was obtained. The EPR spectra are shown in Figure 4 and the parameters used in the simulations of these spectra are shown in Table 3. The EPR spectrum of L386A mutant is quite similar to the wild-type, while the EPR spectrum and the g values, as well as the hyperfine constants of the I494A mutant reveal significant differences in both the T1 and T2 Cu centres. For T1 centre in the I494A mutant, comparing to the spectrum of the wild-type, it is observed an increase in gmax and gmed values and a decrease in gmin value, as well as a decrease in the hyperfine constant value. These observations are compatible with an increase of the distortion of the tetrahedron, which could further accounts for an increase in the Cu-S(Cys) distance, as indicated by the RR results. Interestingly, both EPR and RR data indirectly imply existence of an altered moiety in the proximity of T1 Cu of the I494A mutant. The former, based on a Vanngard-Peisach-Blumberg plot (g_{max} vs. A_{max}), suggests a similarity of the T1 Cu centre of I494A mutant with the T1 Cu site present in blue copper proteins having an oxygen atom as a ligand [36, 37]. The latter data imply, through the weakening of the Cu-S bond, that the T1 Cu ion experiences an extra electron donor interaction from the neighbouring oxygen or possibly an extra polar interaction, which may be sufficient to increase the Cu-S distance substantially [5]. The changes of the g values of T2 Cu in the I494A mutant and the decrease of the A_{max} value, approaching values typical for T1 Cu centres, reflect an increase in tetrahedral distortion of the T2 site. Thus, the mutation of I494 in the vicinity of T1 Cu site seems to cause a perturbation in the trinuclear centre as monitored by EPR and absorption (see above). The T1 Cu site is around 13Å away from the trinuclear centre and is bridged through the T1 Cu-Cys-His-T3 Cu backbone, a possible

efficient pathway for rapid intramolecular electron transfer [1-4]. Therefore, taken into consideration the structural and functional closeness, it is reasonable to assume that drastic modifications of the T1 Cu site in I494A mutant, such as a lower covalency of the T1 Cu-S Cys bond, could lead to alterations in the properties of the trinuclear centre.

Structural Characterization of CotA-mutants.

The modifications of the T1 Cu site geometry in I494A and L386A mutants are clearly confirmed by the X-ray crystallography as shown in Figures 5A and 5B. In the case of the L386A mutant, the T1 Cu ion is barely perturbed, being coordinated by three strong ligands (Cys492 and His419 and 497) at distances of around 2.1Å, with a fourth weaker ligand, Met502 at a distance of 3.2Å. However, in the case of the I494A mutant the reduction in the size of the 494 residue increases the accessibility of the T1 Cu site such that a solvent molecule is able to interact with the Cu ion at a distance of around 3.0Å. The coordination geometry thus changes from distorted tetrahedral in the cases of the Wt protein and the L386A mutant to distorted trigonal bipyramidal in the I494A mutant. The solvent molecule itself is part of a chain of hydrogen bonded water molecules leading to the external surface of the molecule. The resolution of the X-ray data does not, however, permit the observation of any significant change in the Cu-S bond length and therefore the strength of the bond. It therefore cannot substantiate the RR and EPR in this context. Quantitatively, the increase in accessibility [38] of the T1 Cu site is ca. 418.8 $Å^2$. Concomitantly, the accessibility of the site to substrate molecules should also be increased, thus affecting the catalytic properties of this mutant. In addition, the X-ray structural data do not indicate any significant changes in the geometry of the T2 copper centre as indicated by the spectroscopic data. However, there has to be some flexibility at this centre in order for the water molecules, resulting from reduction of dioxygen, to access the exit solvent channel and a concomitant movement of the T2 copper may be reflected by the EPR data. Further, the presence of the dioxygen molecule bisecting the T3 copper ions and with the O2 atom only some 2.5 Å distant from the T2 copper may also have some effect. Changes in its spin state in the I494A mutant may be reflected in the EPR spectra for the T2 copper ion.

In the case of the L386A mutant, two crystal structures have been evaluated, one for a “fully loaded” Cu sample at the medium resolution of 2.9Å and the second for a sample significantly depleted in T2 and 3 Cu ions, but at the improved resolution of 2.4 Å. Despite differences in Cu content within the trinuclear cluster, the two L386A mutant structures are remarkably similar. There are differences in the solvent structure, but these are mainly related to the differences in the resolution of the respective data sets and consequently revealed by the respective electron density maps in details. Thus, in the fully loaded L386A data set only 44 solvent molecules have been modeled. However, since the structure of the Cu depleted L386A mutant extends to a significantly higher resolution than the Cu fully loaded structure and there appear to be no essential differences with respect to the Cu centres, this structure can be used to provide a better definition of the T1 Cu site. The geometry of the trinuclear Cu centre in both the I494A and depleted L386A mutants is essentially the same as that found previously in the native structure (see for example [7]) with the optimum model incorporating a dioxygen species in between the two T3 Cu atoms and almost perpendicular to their connecting vector. The presence of an oxidised cysteine residue at position 35 in the fully loaded structures is surprising and is likely to arise from the production protocol, since intense efforts have been made to minimize and to monitor radiation damage during the data collection procedures. Apart from the T1 Cu centre and

residue 35, the mutant enzymes show no significant structural changes with respect to the Wt enzyme.

Redox properties of the mutants

The reduction of the T1 Cu ion was measured by the disappearance of the CT absorption band in the 500–800 nm regions. The redox potentials of the T1 Cu site were determined to be 525, 429 and 466 mV for the Wt protein and the I494A and L386A mutants, respectively (Table 4). These results indicate that the geometry changes at the active site have led to a stabilization of the Cu(II) form of both mutants. The Cu-S(Cys) bond strength, which can be extracted from the RR spectra, was shown to have a direct correlation with the redox potential of T1 Cu sites [1, 5]. The RR data qualitatively reproduce the experimental findings; an increase in the Cu-S(Cys) bond length for the I494A mutant and a less pronounced lengthening in the case of the L386A mutant, accounting for lowering of the redox potential of both mutants, compared to Wt.

In order to understand the physical reasons behind the changes in the redox potential, simulations of redox behaviour of the Wt and mutant proteins were performed, using the data of the solved X-ray structures. The calculations indicate lower redox potentials for the two mutants, when compared with the Wt, 516 mV for I494A and 510 mV for L386A. This results from a higher exposure to the solvent of the T1 Cu centre in the mutants which stabilises the oxidised state. In fact, given that the overall formal charge of the centre is +1, this is more likely to occur in a medium of higher dielectric constant such as water, than on a low dielectric, such as protein. The lowering of the redox potential of the mutants obtained from the calculations is not as pronounced as that observed experimentally (see above). The discrepancies may arise partially from the use of a somewhat 'unphysical' protein dielectric constant. A dielectric constant of 10 may be adequate for protonatable groups, but does not always describe the redox centres sufficiently well, specifically if they are more buried in the protein [26]. A lower protein dielectric constant results in a larger difference, but the calculation would not be as accurate for protonatable groups which may have a strong effect on nearby redox centres. For instance, calculations with an internal dielectric constant of 4 (data not shown), result in larger differences between the mutants and the Wt. Moreover, the calculations evidence a lower decrease of the redox potential for I494A than for L386A, when compared with the Wt, in disagreement with the experiment. For the I494A mutant, the presence of the additional water molecule at the T1 Cu site cannot be properly handled by the current methodologies due to its most likely quantum mechanical nature, which goes beyond a simple solvation effect (as our calculations would model it). Nevertheless, and in a qualitative way, the water molecule, by orienting the negative oxygen atom towards the Cu ion will likely stabilise the positive oxidised state, thereby decreasing the redox potential even more than evidenced by the calculations presented here. Despite the fact that our calculations are not able to model this in full extent, they show, by comparison of the results obtained for the two mutants, that this effect is an important one, since it can change substantially what could be obtained by unspecific solvation effects.

Catalytic properties of mutant enzymes

Three substrates, one non-phenolic (ABTS) and two phenolic (2,6-DMP and SGZ) were used to determine specific changes of the catalytic properties of the mutant enzymes. Table 4 shows that I494A and L386A mutants have higher values for the K_m and lower k_{cat} values when compared to the Wt enzyme. The L386A mutant exhibits a ca. two-fold increase in the K_m for all tested substrates and a two- to six-fold decrease of k_{cat} values. The I494A mutant is more severely

compromised in its catalytic activity. Major alterations on the enzyme affinity for different substrates were observed (up to 20-fold higher K_m values as compared to Wt) indicating that this mutation must have caused a change in the substrate-binding pocket, as indicated by X-ray results. In addition, significant changes were found for the values of k_{cat}; a lowering by factor of 10 to nearly 50 for the phenolic and non-phenolic substrates, respectively. The parameter k_{cat} depends on the rate-limiting step in the turnover of multicopper oxidases, which was shown to be the reduction of the T1 Cu site [1]. According to the Marcus theory k_{ET} a major component of the parameter k_{cat}, is dependent on three factors: the donor-acceptor electronic coupling, the reorganization energy and the redox potentials [39]. The lower redox potential determined for both mutants lead to a decreased thermodynamic driving force and thus to a decreased electron transfer rate and hence to lower k_{cat} values. In the case of I494 mutant major alterations of the structure near the T1 Cu site were observed including a higher solvent accessibility. The reduction of this site may therefore require an increase in the reorganization energy, which in turn could result in lower k_{ET} and thus lower k_{cat} [32, 33]. The mutation I494A leads to a shift in the optimal pH by approximately 2.0 units for 2,6-DMP and 1.0 unit for SGZ, towards higher values, but not for ABTS (Figure 6). It has been shown that oxidation of a phenolic substrate depends on its protonation state; the deprotonated phenol has a lower redox potential and, therefore, is more easily oxidised [40]. A careful analysis of the protonation behaviour of nearby groups of the substrate binding pocket in the I494A mutant did not reveal any significant difference in their protonation behaviour compared with the Wt enzyme. Therefore, the altered pH dependence found for phenolic substrates might be attributable to altered protonation equilibrium of the phenolic substrates themselves in the T1 substrate binding pocket of I494A mutant, corroborating the changes at this pocket as revealed by increased K_m values. This effect would not be observed for ABTS because there is no protonation equilibrium for this substrate.

CONCLUDING REMARKS

It is known that the redox potentials exhibited by the T1 Cu sites of laccases span over a broad range of values, from 400 mV for plant laccases to 790 mV for some fungal laccases [1, 4]. The reasons for the wide potential range among laccases are not yet fully understood. Since a high redox potential increases the range of oxidizable substrates and improves the effectiveness and versatility of the enzyme it is important to obtain detailed description of the structure and reactivity of variants in the vicinity of the T1 copper site in order to be able to fine-tune its properties by protein engineering techniques. The redox potential of T1 Cu sites can be influenced by a variety of factors, including the solvent accessibility of the metal centre and the electrostatic interactions between the metal centre and the protein [1]. Most of the site-directed mutagenesis at the T1 Cu site studies has been applied to simple blue Cu proteins (possessing one T1 Cu site) in an effort to elucidate their electron transfer mechanism [1] and the results of a similar approach for multicopper oxidases are yet scarce [6, 32, 41-44]. In this study the crystal structures of I494A and L386A mutants show that substitutions of hydrophobic residues by alanine in the vicinity of T1 Cu site has increased the solvent accessibility, and consequently caused a decrease of the redox potential of the metal centre of both mutants. The larger cavity observed in the I494A mutant allowed for the specific binding of a water molecule to the T1 Cu ion, leading to a change in the coordination geometry of this site, from distorted tetrahedral in the case of Wt and L386A mutant to a more trigonal bipyramidal in the I494A mutant. This resulted in a increased Cu-S(Cys) bond length as observed by RR, and significant differences in the *g*

values and the Cu hyperfine coupling constant of the T1 Cu in the EPR spectra. These geometrical and electronic changes further stabilized the oxidised state of T1 Cu site, resulting in a lower redox potential for I494A enzyme as compared to the L386A mutant. As expected, the lower redox properties of I494A and L386A mutants correlate well with their lower reactivity towards standard substrates. Therefore, these results and our previous data [6] show that changes in amino acid residues in direct contact to the metal centre (including ligands) significantly affect the properties of T1 Cu sites of laccases and suggest that modulation of redox potential without compromising the overall reactivity may be performed through changes in residues away from this immediate contact shell.

Acknowledgements

This work was supported by POCI/BIO/57083/2004 and FP6-2004-NMP-NI-4/026456 project grants. The provision of synchrotron radiation facilities and the assistance of the staff at those facilities for help with X-ray data collection are sincerely acknowledged at the European Synchrotron Radiation Facility in Grenoble, France and the Swiss Light Source at the Paul Scherrer Institut, Villigen, Switzerland. Z. Chen holds a FCT Post-doc fellowship (SFRH/BPD/27104/2006).

REFERENCES

1. Solomon, E.I., Sundaram, U.M. and Machonkin, T.E. (1996) Multicopper oxidases and oxygenases. Chem. Ver. **96**, 2563-2605.
2. Messerschmidt, A. (1997). *Multicopper oxidases* (A. Messerschmidt, eds.). Singapore: World Scientific.
3. Lindley, P.F. (2001) Multi-copper oxidases. In Handbook on Metalloproteins. (Bertini I., Sigel, A. and Sigel, H., eds) pp. 763-811, Marcel Dekker, Inc., New York
4. Stoj, C.S., and Kosman, D.J. (2005) Copper proteins: Oxidases. In Encyclopedia of Inorganic Chemistry Vol II, 2nd Ed. (King, R.B., ed). pp. 1134-1159, John Wiley & Sons
5. Blair, D.F., Campbell, G.W., Schoonover, J.R., Chan, S.I., Gray, H.B., Malmstrm, B.G., Pecht, I., Swanson, B.I., Wooddruff, W.H., Cho, W.K., English, A.M., Fry, H.A., Lum, V. and Norton, K.A. (1985) Resonance raman studies of blue copper proteins: effect of temperature and isotopic substitutions. Structural and thermodynamic implications. J. Am. Chem. Soc., **107**, 5755-5756
6. Durão, P., Bento, I., Fernandes, A.T., Melo, E.P., Lindley, P.F. and Martins, L.O. (2006) Perturbations of the T1 copper site in the CotA laccase from *Bacillus subtilis*: structural, biochemical, enzymatic and stability studies. J. Biol. Inorg. Chem. **11**, 514-526.
7. Bento, I., Martins, L.O., Gato, G.L., Carrondo, M.A., Lindley, P.F. (2005) Dioxygen reduction by multicopper oxidases: a structural perspective. Dalton Transactions **21,** 3507-3513.
8. Enguita, F. J., Marcal, D., Martins, L. O., Grenha, R., Henriques, A. O., Lindley, P. F., and Carrondo, M. A. (2004) Substrate and doxygen binding to the endospore CotA laccase from *Bacillus subtilis*. J. Biol. Chem. 279, 23472-23476.
9. Martins, L.O., Soares, C.M., Pereira, M.M., Teixeira, M., Jones, G.H. and Henriques, A.O. (2002) Molecular and biochemical characterization of a highly stable bacterial laccase that occurs as a structural component of the *Bacillus subtilis* endospore coat. J. Biol. Chem. **277**, 18849-18859.
10. Durão, P., Chen, Z., Fernandes, A.T., Hildebrandt, P., Murgida, D.H., Todorovic, S., Pereira, M.M., Melo, E.P. and Martins, L.O. (2008) Copper incorporation into recombinant CotA laccase from *Bacillus subtilis*: characterization of fully copper loaded enzymes. J. Biol. Inorg. Chem. **13**, 183-193
11. Aasa, R. and Väangard, V.T. (1975) EPR signal intensity and powder shapes: A reexamination. J. Magnet. Reson. **19**, 308-315.
12. Leslie, A.G.W. (2006) The integration of molecular diffraction data. Acta Cryst. D**62**, 48-57.
13. Evans, P. (2006) Scaling and assessment of data quality. Acta Cryst. D**62**:72-82
14. CCP4, (1994) Collaborative Computational Project. Number 4. Acta Cryst. D**50**: 760-763.
15. Vagin, A. and Teplyakov, A. (1997) MOLREP: an Automated Program for Molecular Replacement. J. Appl. Cryst. **30**, 1022-1025.

16. Murshudov, G.N., Vagin, A.A., Lebedev, A., Wilson, K.S. and Dodson, E.J. (1999) Efficient anisotropic refinement of macromolecular structures using FFT. Acta Cryst. D **55**, 247-255.

17. Tronrud, D. (1996) The limits of interpretation. CCP4 Study Weekend Macromolecular Refinement, pp 1-10.

18. Emsley, P. and Cowtan, K. (2004) Coot: model-building tools for molecular graphics. Acta Cryst. D **60**, 2126-2132.

19. Read, R.J. (1986) Improved Fourier coefficients for maps using phases from partial structures with errors. Acta Cryst. A, **42**, 140-149.

20. Baptista, A.M., Teixeira, V.H., and Soares C.M. (2002) Constant-pH molecular dynamics using stochastic titration. J. Chem. Phys. **17**, 4184-4200.

21. Teixeira, V.H., Soares, C.M. and Baptista, A.M. (2002) Studies of the reduction and protonation behaviour of tetrahaem cytochromes using atomic detail. J. Biol. Inorg. Chem. **7**, 200-216.

22. Bashford, D. and Gerwert, K. (1992) Electrostatic calculations of the p*Ka* values of ionizable groups in bacteriorhodopsin. J. Mol. Biol. **224**, 473-486.

23. Bashford, D. (1997) An object-oriented programming suite for electrostatic effects in biological molecules. In: Scientific Computing in Object-Oriented Parallel Environments (Ishikawa, Y., Oldehoeft, R.R., Reynders, J.V.W., Tholburn, M., eds). pp 233-240 Springer Berlin: ISCOPE97

24. Scott, W.R.P., Hünenberger, P.H., Tironi, I.G., Mark, A.E., Billeter, S.R., Fennen, J., Torda, A.E., Huber, T., Krüger, P. and van Gunsteren, W.F. (1999) The GROMOS biomolecular simulation program package. J. Phys. Chem. **103**, 3596-3607.

25. van Gunsteren, W.F., Billeter, S.R., Eising, A.A., Hunenberger, P.H., Kruger, P., Mark, A.E., Scott, W.R.P. and Tironi, I.G. (1996) Biomolecular simulation: The GROMOS96 manual and user guide. Zurich, Groninger: BIOMOS b.v.

26. Teixeira, V.H., Cunha, C.A., Machuqueiro, M., Oliveira, A.S., Victor, B.L., Soares, C.M. and Baptista, A.M (2005) On the use of different dielectric constants for computing individual and pairwise terms in poisson-boltzmann studies of protein ionization equilibrium. J Phys Chem B Condens Matter Mater Surf Interfaces Biophys **109**, 14691-706.

27. Frisch, M.J., Trucks, G.W., Schlegel, H.B., Scuseria, G.E. Robb, M.A., Cheeseman, J.R., Zakrzewski, V.G. Montgomery, J., Stratmann, R.E., Burant, J.C. Dapprich, S., Milliam, J.M., et al. 1998. Gaussian 98, Revision A.7. Pittsburgh PA: Gaussian, Inc.

28. Bayly, C.I., Cieplak, P., Cornell, W.D. and Kollman, P.A. (1993) A well-behaved electrostatic potential based method using charge restraints for deriving atomic charges: the RESP model. J. Phys. Chem. **97**,10269-10280.

29. Brenner, AJ, Harris, ED (1995) A quantitative test for copper using bicinchoninic acid. Anal Biochem **226,** 80-84.

30. Bradford, M.M. (1976) A rapid and sensitive method for the quantification of microgram quantities of protein utilizing the principle of protein-dye binding. Anal. Biochem. **72**, 248-254.

31. Dave, B.C., Germanas, J.P. and Czernuszewicz, R.S. (1993) The first direct evidence for copper(II)-cysteine vibrations in blue copper proteins: resonance raman spectra of ^{34}S-Cys-labeled azurins reveal correlation of copper-sulfur stretching frequency with metal site geometry. J Am Chem Soc **115**, 12175-12176.

32. Palmer, A.E., Randall, D.W., Xu, F. and Solomon, E.I. (1999) Spectroscopic studies and electronic structure description of the high potential Type 1 copper site in fungal laccase: insight into the effect of the axial ligand. J Am Chem Soc **121**, 7138-7149

33. Machonkin, T.E., Quintanar, L., Palmer, A.E., Hassett, R., Severance, S., Kosman, D.J. and Solomon, E.I. (2001) Spectroscopy and reactivity of the Type 1 copper site in Fet3p from *Saccharomyces cerevisiae*: correlation of structure with reactivity in the multicopper oxidases. J Am Chem Soc **123**, 5507-5517

34. Green, M.T. (2006) Application of badger's rule to heme and non-heme iron-oxygen bonds: an examination of ferryl protonation states. J Am Chem Soc **128**, 1902-1906.

35. Qiu, D., Dong, S., Ybe, J., Hecht, M. and Spiro, T.M. (1995) Variations in the Type 1 copper protein coordination group: resonance raman spectrum of ^{34}S-, ^{65}Cu-, and ^{15}N-labeled plastocyanin. J Am Chem Soc **117**, 6443-6446.

36. Andrew, C. R., Yeom, H., Valentine, J. S., Karlsson, B. G, Bonander, N., Pouderoyen, G., Canters, G. W., Loehr, T. M. and Sanders-Loehr, J. (1994) *J. Am. Chem. Soc.* 116, 11489-11498.

37. Diederix, R. E. M., Canters, G. W. and Dennison, C. (2000) *Biochemistry* 39, 9551-9560.

38. Binkowski, T.A., Naghibzadeh, S. and Liang, J. (2003) CASTp: Computed atlas of surface topography of proteins. Nucleic Acids Res. **31**, 3352-3355.

39. Moser, C.C. and Dutton, P.L. (1996) In: Protein electron transfer. (Bendall, D.S., ed.) pp. 1-21 Bios Scientific Publishers Ltd

40. Xu, F. (1997) Effects of redox potential and hydroxide inhibition on the pH activity profile of fungal laccases. J. Biol. Chem. **272**, 924-928.

41. Xu, F., Berka, R.M., Wahleithner, J.A., Nelson, B. A., Shuster, J. R., Brown, S. H., Palmer, A. E. and Solomon, E. I. (1998) Site-directed mutations in fungal laccase: effect on redox potential, activity and pH profile. Biochem. J. **334**, 63-70.

42. Xu, F., Palmer, A. E., Yaver, D. S., Berka, R. M., Gambeta, G. A., Brown, S. H. and Solomon, E. I. (1999) Targeted mutations in a *Trametes villosa* laccase. Axial perturbation of the T1 copper. J. Biol. Chem. **274**, 12372-12375.

43. Palmer, A. E., Szilagyi, R. K., Cherry, J. R., Jones, A., Xu, F. and Solomon, E. I. (2003) Spectroscopic characterization of the Leu513His variant of fungal laccase: effect of increased ligand interaction on the geometric and electronic structure of the Type 1 Cu site. Inorg. Chem. **42**, 4006-4017.

44. Madzak, C., Mimmi, M.C., Caminade, E., Brault, A., Baumberger, S., Briozzo, P., Mougin, C. and Jolivalt, C. (2006) Shifting the optimal pH of activity for a laccase from the fungus *Trametes versicolor* by structure-based mutagenesis. Prot Eng, Design & Selection **19**, 77-84.

FIGURE LEGENDS

Figure 1. Structural detail of the T1 Cu site in the native CotA-laccase structure showing the hydrophobic I494 and L386 residues [7].

Figure 2. UV-Visible spectra of Wt CotA (solid thin line), L386A mutant (solid thick line) and I494A mutant (dashed line).

Figure 3. RR spectra of the Wt CotA (a), L386A mutant (b) and I484A mutant (c), obtained with 567.9 nm excitation and 5mW laser power at 77K, accumulation time 40s.

Figure 4. EPR spectra of the Wt CotA (a), L386A mutant (b) and I484A (c), obtained at 10 K. Microwave frequency, 9.39 GHz 2.4 mW; modulation amplitude: 0.9 mT.

Figure 5. Structure of the T1 Cu centre in the L386A mutant (a) and I494A mutant (b).

Figure 6. pH profile for catalytic activities using as substrates ABTS (a), 2,6-DMP (b) and SGZ (c) for Wt CotA (○), I494A mutant (□) and L386A mutant (Δ).

Table 1. X-ray Data Collection.

	I494A	L386A-fully Cu loaded	L386A-Cu depleted
Synchrotron Beam line	ESRF* ID14-3	ESRF* ID14-2	SLS† X06FA
Wavelength (Å)	0.931	0.933	0.9184
Detector Distance (mm)	150.4	275.5	250
Resolution (Å)	1.6	2.9	2.4
Space group	P3121	P3121	P3121
Cell parameters a (Å) c	101.87 137.04	101.78 137.12	101.96 136.14
Mosaicity (°)	0.44	0.55	0.53
Oscillation range (°)	0.3	0.8	1.0
Oscillation angle (°)	90	96	90
No. of unique *hkl* †	107969 (15440)	107199 (15756)	180374 (26244)
Completeness (%) †	99.4 (98.4)	100.0 (100.0)	100.0 (100.0)
I/σ(I) †	6.9 (2.1)	6.2 (2.3)	5.5 (5.6)
R_{symm} †	0.064 (0.346)	0.100 (0.315)	0.076 (0.32)
Multiplicity †	5.2 (3.9)	5.7 (5.8)	5.5 (5.6)

† Values in parentheses refer to the highest resolution shells as follow;

I494A	1.69 – 1.60 Å
L386A - fully Cu loaded	3.06 – 2.90 Å
L386A – Cu depleted	2.53 – 2.40 Å

* European Synchrotron Radiation Facility, Grenoble, France.

† Swiss Light Source, Paul Scherrer Institut, Villigen, Switzerland.

Table 2. Cu content and spectral properties for the Wt CotA and I494A and L386A mutants.

	Cu content (mol Cu/mol prot)	**T1 λ (ε)**	**T3 λ (ε)**
CotA Wt	3.7 ± 0.1	609 (4.0)	330 (4.0)
L386A	4.0 ± 0.2	609 (3.3)	330 (3.0)
I494A	4.0 ± 0.2	624 (5.6)	330 (1.5)

Units are: **λ, nm, ε, $mM^{-1}cm^{-1}$**

Table 3. EPR parameters used in the simulation of Wt CotA, L386A and I494 mutants spectra.

	Cu centers	g_{min}	g_{med}	g_{max}	A_{max} ($\times 10^{-4}$ cm^{-1})
CotA Wt	T1	2.044	2.052	2.230	64
	T2	2.025	2.099	2.255	179
L386A	T1	2.046	2.048	2.235	64
	T2	2.025	2.095	2.258	174
I494A	T1	2.038	2.068	2.305	45
	T2	2.055	2.102	2.347	93

Table 4. Redox potential and kinetic constants of the Wt CotA laccase and L386A and I494A mutants. The redox potentials were measured at pH 7.6. The kinetic constants were measured at the optimal pH for the different substrates for each variant enzyme (see Figure 6).

		ABTS			2,6-DMP			SGZ		
	***E*° (mV)**	K_m (μM)	k_{cat} (s^{-1})	k_{cat}/K_m ($s^{-1}\mu M^{-1}$)	K_m (μM)	k_{cat} (s^{-1})	k_{cat}/K_m ($s^{-1}\mu M^{-1}$)	K_m (μM)	k_{cat} (s^{-1})	k_{cat}/K_m ($s^{-1}\mu M^{-1}$)
CotA Wt	525 ± 10	124 ± 17	322 ± 20	2.6	227 ± 41	36 ± 5	0.16	18 ± 3	80 ± 4	4.4
L386A	466 ± 6	145 ± 3	52 ± 1	0.36	576 ± 16	17.0 ± 0.3	0.03	33 ± 1	13 ± 0.2	0.39
I494A	429 ± 27	2027 ± 193	7.2 ± 0.5	0.0036	1295 ± 73	4.5 ± 0.2	0.0035	52 ± 1	9 ± 0.1	0.17

Durão et al.

Figure 1

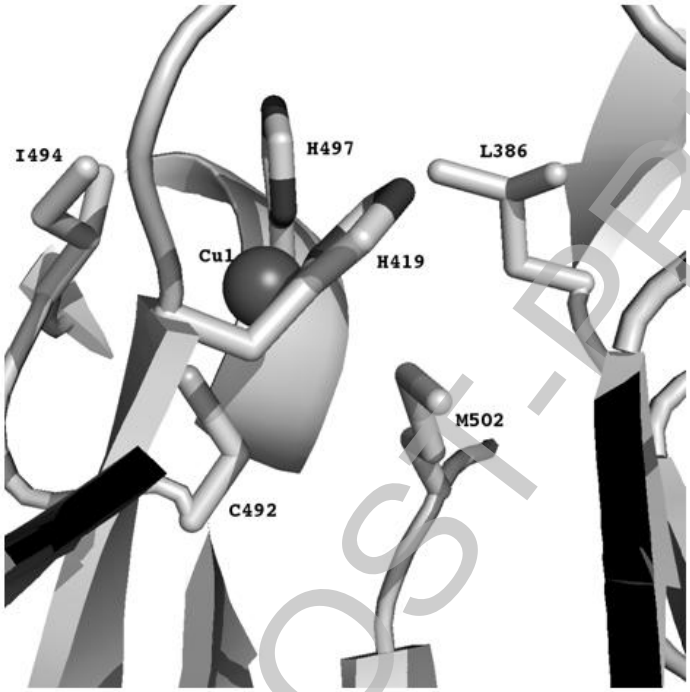

Durão et al.

Figure 2

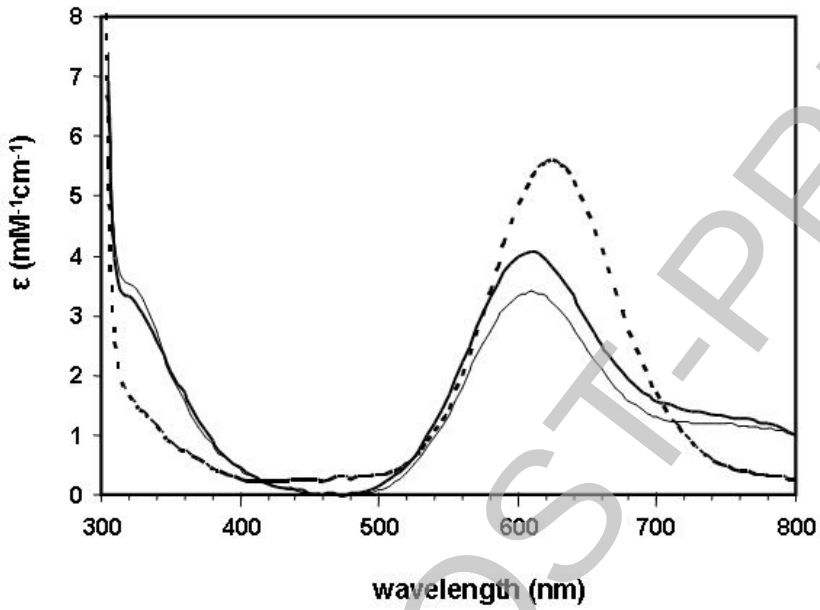

Durão et al.

Figure 3

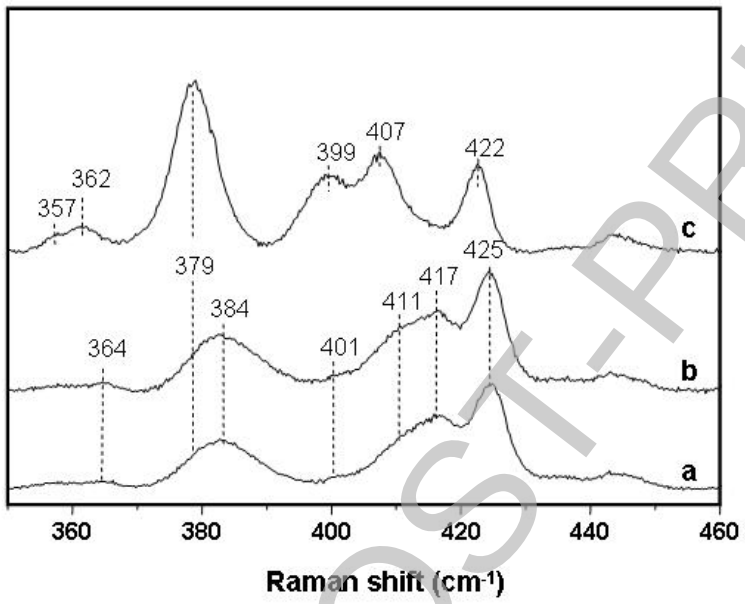

Durão et al.

Figure 4

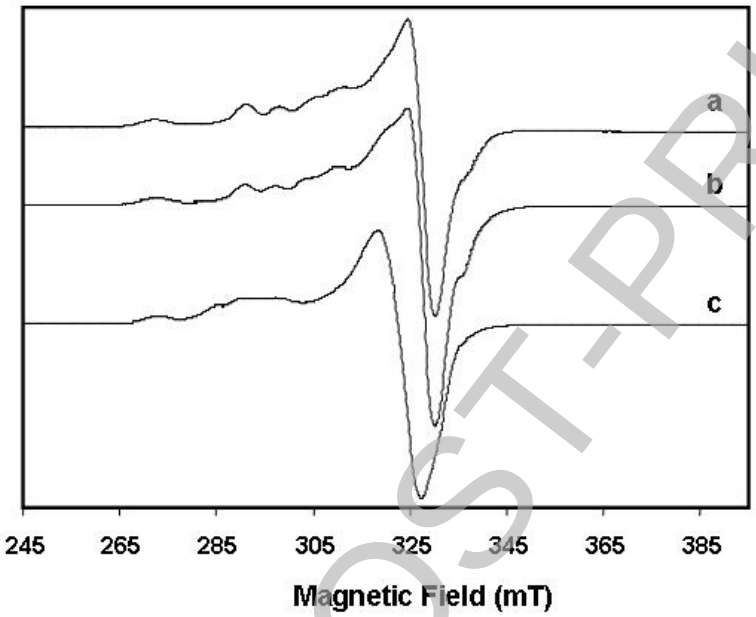

Durão et al.

Figure 5

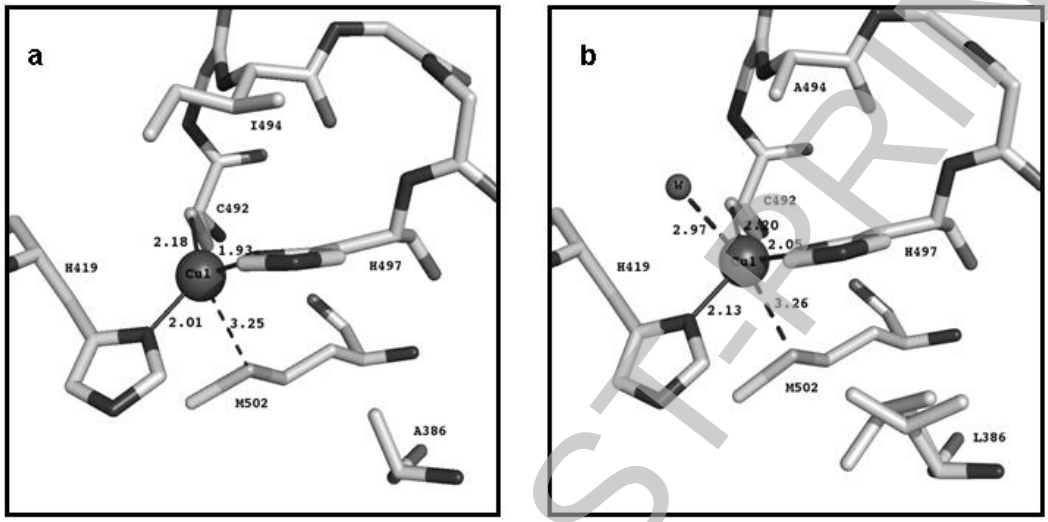

Durão et al.

Figure 6